Engineering Structures 255 (2022) 113903

Contents lists available at ScienceDirect

Engineering Structures

journal homepage: www.elsevier.com/locate/engstruct

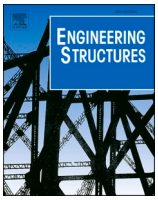

Explainable machine learning model and reliability analysis for flexural capacity prediction of RC beams strengthened in flexure with FRCM

Tadesse G. Wakjira [a,b], Mohamed Ibrahim [a], Usama Ebead [a,*], M. Shahria Alam [b]

[a] Department of Civil and Architectural Engineering, College of Engineering, Qatar University, P.O. Box 2713, Doha, Qatar
[b] Applied Laboratory for Advanced Materials & Structures (ALAMS), School of Engineering, The University of British Columbia, Kelowna, BC V1V 1V7, Canada

ARTICLE INFO

Keywords:
FRCM
Machine learning
SHAP
Reliability analysis
Strengthening

ABSTRACT

This paper presents a data-driven approach to determine the load and flexural capacities of reinforced concrete (RC) beams strengthened with fabric reinforced cementitious matrix (FRCM) composites in flexure. A total of seven machine learning (ML) models such as kernel ridge regression, K-nearest neighbors, support vector regression, classification and regression trees, random forest, gradient boosted trees, and extreme gradient boosting (xgBoost) are evaluated to propose the best predictive model for FRCM-strengthened beams. Beam geometry, internal steel reinforcement area, FRCM reinforcement area, and mechanical characteristics of concrete, steel, and FRCM are the main input parameters included in the database. Among the studied ML models, the xgBoost model is the most accurate model with the highest coefficient of determination (R^2 = 99.3%) and least root mean square (RMSE), mean absolute error (MAE), and mean absolute percentage error (MAPE). A comparative study of the performance of the proposed and existing analytical models revealed the superior predictive capability and robustness of the proposed model. The predicted flexural and load capacities of the beams based on the existing analytical models are highly scattered and either over-conservative or unsafe. A unified SHapley Additive exPlanations approach is employed to explain the output of the best ML model and identify the most significant input features and interactions that influence the capacity of FRCM-strengthened RC beams in flexure. Furthermore, a reliability analysis is performed to calibrate the resistance reduction factor (ϕ) to achieve a specified target reliability index (β_T = 3.5).

1. Introduction

The strengthening of reinforced concrete (RC) structures is becoming a crucial part of construction activities due to several factors that lead to structural deterioration. These factors include corrosion of reinforcement bars, obsolete design, and improper maintenance among other factors. Thus, efficient repair and strengthening systems are required to restore or even improve the capacity of deteriorated structures and extend their life spans. In this context, fabric reinforced cementitious matrix (FRCM) composites have recently gained immense attention owing to their favorable advantages over traditional strengthening systems [1,2]. Successful applications of the FRCM have been reported for the strengthening of RC slabs [3], RC beams [4–27], RC columns [28–31], and masonry structures [32–36].

With regard to the FRCM-strengthened RC beams, a considerable amount of research effort has been allotted to experimentally investigate their flexural behavior [4–7,14–18,21–27]. The behavior of RC beams strengthened in flexure using FRCM is mainly governed by the debonding of the FRCM system off the concrete substrate [37]. Different analytical models have been proposed in an attempt to determine the effective strains in the strengthening systems at debonding and consequently, the flexural capacity of the strengthened beams [37–42]. However, most of these models were originally developed for the fiber reinforced polymer (FRP) strengthening system and adopted to the FRCM [39–41], despite the difference in the response behavior between FRP and FRCM under the applied load. Besides, there exist significant discrepancies in the prediction capability of the existing models as these models were empirically developed based on the predefined formulas and experimental datasets mainly generated for a limited number of input parameters. Hence, it is vital to develop a reliable and accurate model for estimating the load and flexural capacities of the FRCM-strengthened RC beams and achieve a safe and economical retrofitting design.

Recently, machine learning (ML) algorithms have emerged as a

* Corresponding author.
E-mail address: uebead@qu.edu.qa (U. Ebead).

https://doi.org/10.1016/j.engstruct.2022.113903
Received 22 August 2021; Received in revised form 23 December 2021; Accepted 13 January 2022
Available online 24 January 2022

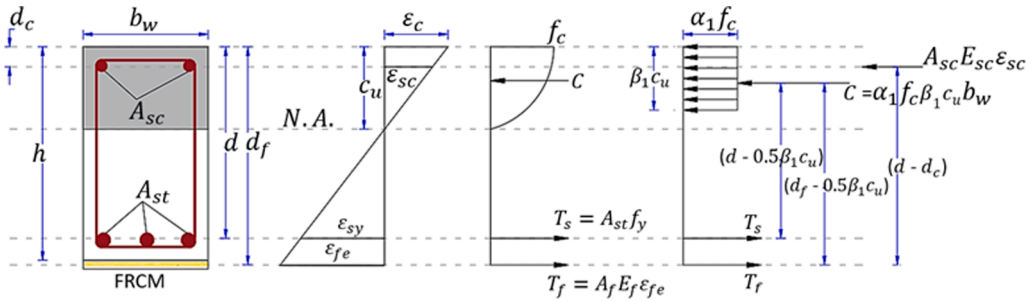

Fig. 1. Cross-section and internal stress and strain distribution of RC beams strengthened with FRCM in flexure.

powerful technique to solve different civil engineering problems [43–53]. This is attributed to their ability to estimate the relationship between the factors and the response parameter(s) without the requirement for prior assumptions of the underlying mathematical and physical models, contrasting to most empirical models [54]. Some of the applications of ML techniques reported in the literature include the prediction of mechanical properties of concrete [44,46–48], load capacity and failure modes of RC columns and walls [49,55,56], shear [57–61] and torsional [62] capacities of RC beams, and seismic damage assessment of RC buildings and bridges [63–65].

Moreover, successful applications of different ML techniques such as genetic algorithm (GA) and artificial neural network (ANN) have been reported in the literature to estimate the load capacity of FRP-strengthened RC beams [66–69]. Perera et al. [66] applied ANN and GA to estimate the shear capacity of RC beams strengthened with externally bonded (EB) FRP. The predicted shear capacities of the strengthened beams were in acceptable agreement with the corresponding experimental results. They investigated the effects of the beam cross-sectional dimensions, modulus of elasticity of the FRP, yield strength of steel reinforcement, areas of steel reinforcement and FRP, inclination of the principal FRP fibers, and concrete compressive strength. A dataset comprised of only 46 RC beams strengthened with EB-FRP was considered in the developed models [66]. Tanarslan et al. [67] developed an ANN model based on a larger database of 84 specimens to estimate the shear capacity of RC beams strengthened with EB-FRP. Moreover, they considered the effects of the shear span-to-depth ratio and different strengthening configurations for the first time [67]. It was concluded that the developed model resulted in a higher prediction capability compared to the existing code equations. Similarly, other studies showed the efficacy of ML models for estimating the shear capacity of RC beams strengthened with EB-FRP sheets [67,69] and near surface mounted FRP rods [68].

Despite the promising results of the applications of ML techniques in this regard, the literature lacks to report its application for estimating the response of RC beams strengthened with FRCM. Moreover, ML models are mostly considered as 'black boxes'; thus, the explainability of ML models is an imperative step to support the output of a given ML model. In this regard, a unified SHapley Additive exPlanations (SHAP) approach has been proposed by Lundberg and Lee [70] to explain the output of any machine learning model. However, only limited studies have explored the explainability of ML-based models applied to the structural engineering field [71–74]. Therefore, this paper presents a pioneer explainable and reliable ML-based model for predicting the flexural capacity of strengthened RC beams with FRCM. The paper also presents a review of the existing analytical models. The developed ML models are compared with the existing models and guideline equations. Finally, a reliability analysis is performed to calibrate the resistance reduction factor to achieve a specified target reliability index. Thus, the research presented in this study is aimed to address the following aspects:

- Develop accurate and reliable ML model for determining the flexural capacity of flexural strengthened RC beams using different FRCM types;
- Compare the prediction accuracy of the developed model against that of the existing analytical models;
- Investigate the output of ML model and rank the input features and their interactions that influence the load and flexural capacity of FRCM-strengthened RC beams in flexure using the unified SHAP approach; and
- Calibrate a resistance reduction factor to achieve a specified target reliability index of the developed model based on reliability analysis.

2. Existing models

In existing formulae, a cross-sectional model was adopted to estimate the nominal flexural capacity (M_n) of FRCM-strengthened RC beams [42]. From the equilibrium of stresses in Fig. 1, the flexural capacity of an FRCM-strengthened RC beam can be given by:

$$M_n = A_{st} f_y \left(d - \frac{\beta_1 c_u}{2}\right) + A_{sc} E_{sc} \varepsilon_{sc} \left(\frac{\beta_1 c_u}{2} - d_c\right) + A_f E_f \varepsilon_{fe} \left(d_f - \frac{\beta_1 c_u}{2}\right) \quad (1)$$

where,

A_{sc} and A_{st} are the reinforcement area of compressive and tensile steel bars, respectively,
β_1 is the concrete stress block parameter (Fig. 1),
d and d_c are the distance between the extreme fiber of the beam and the center of the tensile and compressive steel bars, respectively, (Fig. 1),
c_u is the neutral axis depth (Fig. 1),
f_y is the yield strength of internal steel reinforcement bars,
E_{sc} and ε_{sc} are the elastic modulus and tensile strain of the compressive reinforcement bars, and
d_f, A_f, E_f, and ε_{fe} are the effective depth, reinforcement area, elastic modulus, and effective strain of the FRCM reinforcement.

According to Bencardino et al. [37], Eq. (1) can be approximated as shown in Eq. (2) with the following three assumptions: (a) the tensile reinforcement bars reached their yielding point at the ultimate load, (b) the strains in the FRCM is equal to the debonding strain ($\varepsilon_{fe} = \varepsilon_{deb}$), and the moment arms of the steel reinforcement and FRCM are equal to 90% of the effective depth and height of the beam, respectively.

$$M_n = 0.9 d A_{st} f_y + 0.9 h E_f A_f \varepsilon_{deb} \quad (2)$$

where h is the cross-sectional height of the beam. The load capacity of the FRCM-strengthened beams can then be determined based on the loading configuration. It is worth mentioning here that this simplified equation does not consider the contribution of compressive reinforcement bars.

The available models for the flexural capacity of RC beams strengthened with FRCM vary mainly in the formulations for estimating

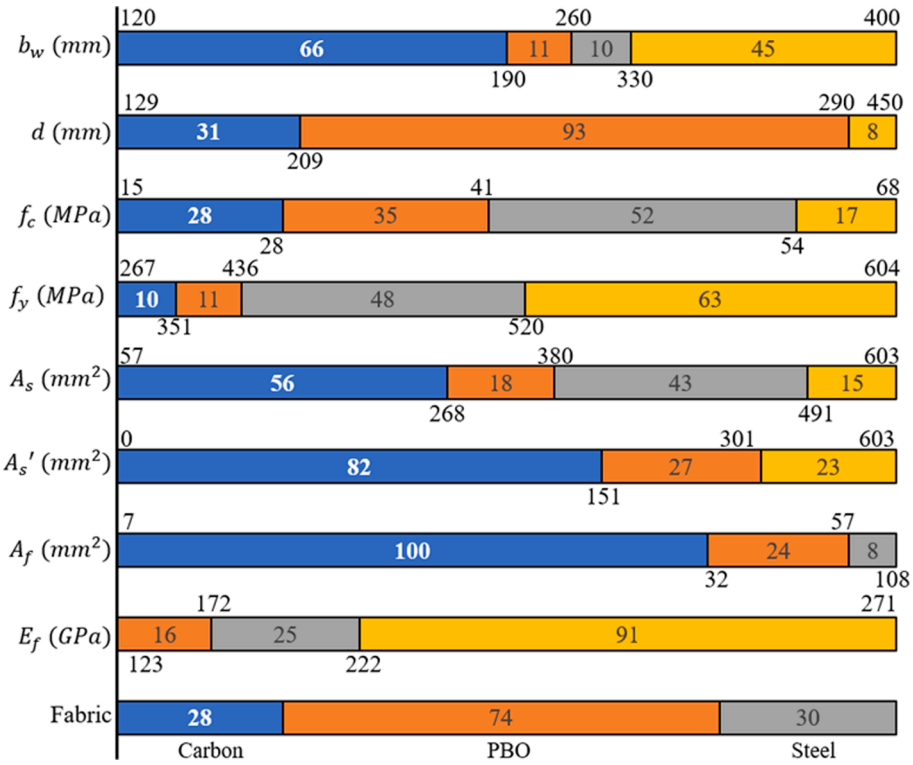

Fig. 2. Distribution of the input variables.

the values of debonding strains, ε_{deb}. Five models adopted in the literature for determining the effective/debonding strain in the FRCM reinforcement are discussed below.

2.1. Model-1: Jung et al. [42]

Jung et al. [42] suggested the following expression for the debonding strain of FRCM composite based on the Teng et al. [75] model, originally proposed for FRP system:

$$\varepsilon_{deb} = \alpha_p \beta_w \beta_L \sqrt{\frac{E_f \sqrt{f_c}}{t_p \sqrt{n_f}}} \tag{3}$$

$$t_p = t_f \times \sqrt{n_f} \tag{3a}$$

$$\beta_W = \sqrt{\frac{2 - b_f/b_w}{1 + b_f/b_w}} \tag{3b}$$

$$\beta_L = \begin{cases} 1, L_f \geq L_e \\ \sin\dfrac{\pi L_f}{2L_e}, L_f < L_e \end{cases} \tag{3c}$$

$$L_e = \sqrt{\frac{E_f t_P}{\sqrt{f_c}}} \tag{3d}$$

where α_p is a coefficient that is experimentally calibrated to be 0.729, f_c is the compressive strength of concrete, b_w is width of the beam section, b_f is the width of the bonded plate, t_f is the fabric thickness, n_f is the number of layers, and L_f is the bond length.

2.2. Model-2: Bencardino et al. [37]

Bencardino et al. [37] suggested the following empirical equation for determining ε_{deb} based on the results of a nonlinear regression analysis for steel FRCM strengthened beams.

$$\varepsilon_{deb} = 2.24\left(E_f t_f\right)^{-0.52} \tag{4}$$

They also used the fracture mechanics approach to come up with another formula as shown in Eq. (5).

$$\varepsilon_{deb} = K\sqrt{2G_f}\sqrt{\frac{1}{t_f E_f}} \tag{5}$$

where G_f is the fracture energy at the debonding surface. It is required to perform flexural tests on RC beams in addition to single/double shear test for the FRCM to determine the coefficient K, which limits the application of this equation in determining ε_{deb}. Thus, only Eq. (4) is adopted in this study.

2.3. Model-3: Ceroni and Salzano [76]

Ceroni and Salzano [76] examined the influence of different factors on the debonding strains of FRCM systems based on the results of 856 single and double shear tests on concrete (347) and masonry (509) elements bonded externally with FRCM. Based on the results of a nonlinear regression analysis on the collected data, the authors suggested the following equation to determine the debonding strain in the FRCM system bonded to concrete elements.

$$\varepsilon_{deb} = 0.008\frac{\left(f_c\right)^{1.15}}{\left(E_f A_f\right)^{0.3}} \tag{6}$$

2.4. Model-4: Mandor and El Refai [77]

Mandor and El Refai [77] have recently investigated the debonding strains in the FRCM strengthening system used for flexural members. Based on the results of the sensitivity analysis, axial stiffness of FRCM ($E_f A_f$), compressive strength of the concrete substrate, and tensile strength (f_{ct}) of the concrete substrate were identified as the three most

Table 1
Distribution of input parameters.

Description	Input parameter	Mean	STD	Min	Max	Q1	Q2	Q3
Geometry	b_w (mm)	250.2	115.9	120	400	150	176	400
	d (mm)	218.7	66.24	129	450	210	210	217
Concrete	f_c (MPa)	40.86	14.44	15.1	67.5	29.13	42.38	49.0
Internal reinforcement	f_y (MPa)	496.4	85.13	267	604.2	468.3	517.2	537
	$A_{st}(mm^2)$	331.3	134.1	157	602.9	212.5	339.1	461.6
	$A_{sc}(mm^2)$	159.3	165.3	0.00	602.9	0.00	100.5	157.1
FRCM reinforcement	$A_f(mm^2)$	26.39	18.71	6.75	108	13.80	23.0	31.96
	E_f (GPa)	234.7	48.45	73.5	271	206	270	270
	Fabric type	Carbon, PBO, Steel						

STD: standard deviation; Max: maximum; Min: minimum; and Q1, Q2, Q3: 25th, 50th, and 75th percentiles.

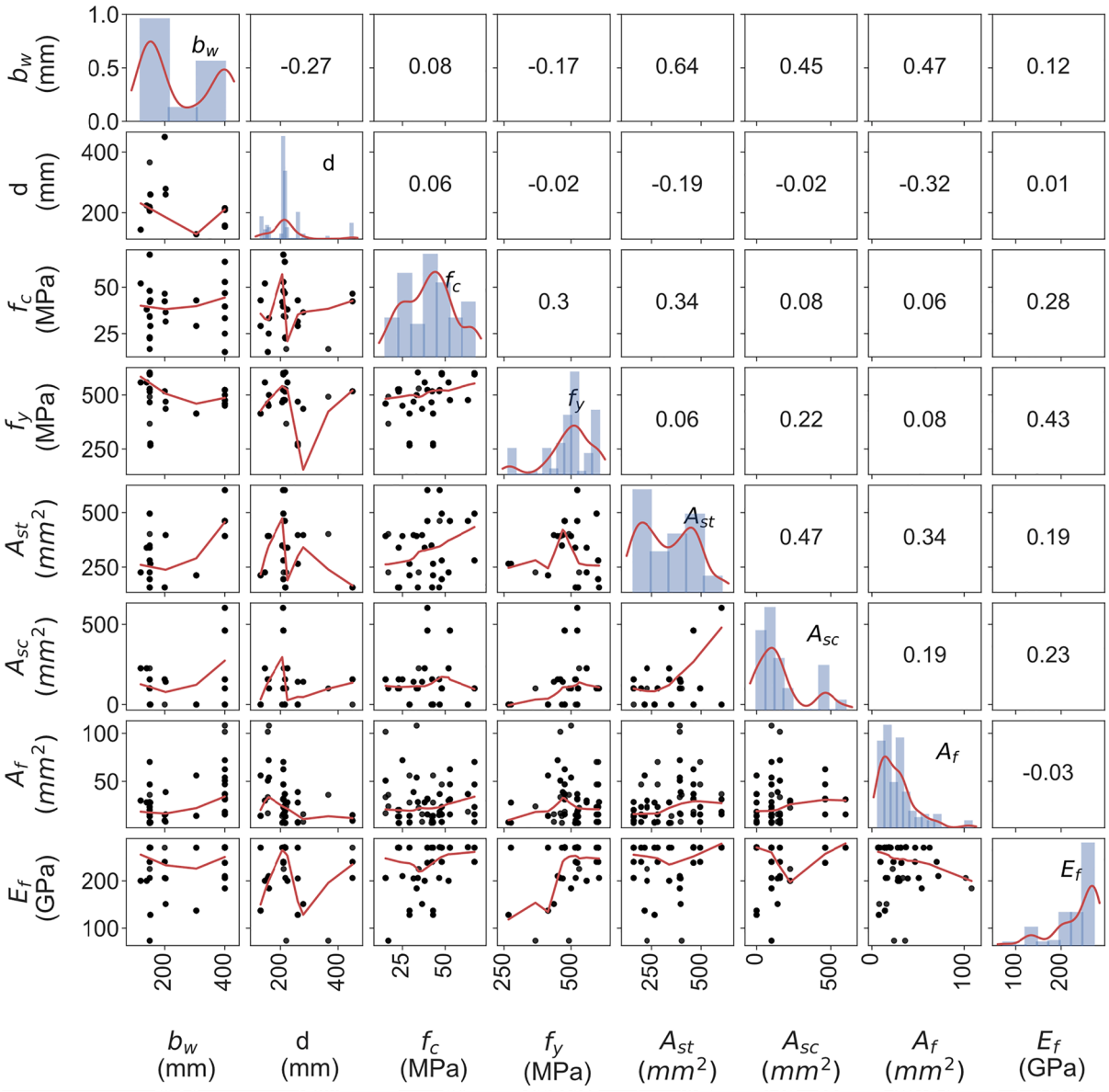

Fig. 3. Details of the dataset used for flexural deficient RC beams strengthened with FRCM.

important factors that influence debonding strains in FRCM. Finally, they proposed three simple optimized models for determining the debonding strains in FRCM, as follows:

$$\varepsilon_{deb} = 0.77 \frac{f_{ct}^{1.191} f_{cm}^{0.056} e^{(0.032 f_c)}}{\left(E_f A_f\right)^{0.091}} \tag{7}$$

$$\varepsilon_{deb} = 0.77\frac{{f_{ct}}^{1.232}e^{(0.035f_c)}}{\left(E_f A_f\right)^{0.083}} \tag{8}$$

$$\varepsilon_{deb} = 0.95\frac{{f_{cm}}^{0.28}e^{(0.056f_c)}}{\left(E_f A_f\right)^{0.153}} \tag{9}$$

where f_{cm} is the compressive strength of FRCM mortar.

In the first equation, the debonding strain is given as the function of the compressive and tensile strengths of concrete, compressive strength of FRCM mortar, and axial stiffness of FRCM. Based on the results of the analysis, the authors concluded that the exclusion of the compressive strength of FRCM mortar has no significant effect on the predicted debonding strains. Among the proposed equations, the first two equations were reported as the best predictive equations, while the third equation showed the least predictive performance. Moreover, the second equation showed the least coefficient of variation (0.26). Hence, the second equation is considered in this study.

2.5. Model-5: ACI549.4-20 model [38]

The ACI 549.4-20 [38] guideline suggests the following expression for determining the value of ε_{deb} interms of the design tensile strain (ε_{fd}) and ultimate tensile strain (ε_{fu}) of the FRCM composite:

$$\varepsilon_{deb} = \varepsilon_{fd} = \varepsilon_{fu} \leq 0.012 \tag{10}$$

The design tensile strain and tensile modulus of the FRCM composite are obtained by testing FRCM coupons. Thus, it is required to perform a test on the FRCM coupons to use this equation. Therefore, this model has been excluded from the current study.

3. Preparation of the dataset and description of input parameters

A database of flexural strengthened rectangular RC beams with FRCM collected from the literature [4–10,16,21–27] is used in this study. A total of 132 RC beams strengthened in flexural with FRCM are included in the developed database. A wide range of beam geometries, mechanical characteristics of materials (concrete, steel, and FRCM), FRCM fabric types (carbon, polyparaphenylene benzobisoxazole (PBO), and steel), and reinforcement areas for both internal steel reinforcement and external FRCM reinforcement are considered in the database, as shown in Fig. 2. However, the mechanical characteristics of FRCM mortar are not reported in most of the studies, thus, its effect on the flexural capacity of the strengthened beam is not considered herein. Different input variables including the width of the web (b_w), effective cross-sectional depth (d), concrete compressive strength (f_c), yield strength of steel bars (f_y), area of steel reinforcement in the tension (A_{st}) and compression (A_{sc}) zones, elastic modulus of FRCM fibers (E_f), number of FRCM fabric layers (n_f), width of FRCM plate (b_f), and thickness of the FRCM fabrics (t_f) are considered in this study. The width of the FRCM plate, the thickness of the fabrics, and the number of FRCM fabric layers are represented in terms of the area of FRCM reinforcement, $A_f = b_f n_f t_f$. Thus, the final input vector comprises a total of nine parameters. It is worth mentioning here that the response of two beams strengthened with an equivalent A_f, but different numbers of fabric layers in FRCM may vary due to the difference in the behavior of the FRCM system with the change in the number of fabric layers. However, the current model does not consider such an effect on the flexural response of the strengthened beams. Table 1 presents the statistical distribution of the input parameters of the experimental database used in this study, while the range of each input variable is clearly illustrated in Fig. 2. In addition, Fig. 3 shows an 8 × 8 matrix in which the diagonal of the matrix shows the histogram for the distribution of each variable, whereas the lower and upper triangular matrices show the scatter plot and Pearson correlation coefficient (r) between the input variables, respectively.

4. Machine learning models

Seven different types of data-driven ML models are evaluated to determine the final best predictive model for the flexural capacity of FRCM-strengthened RC beams in flexure. In the proposed ML models, the flexural capacity of the strengthened beams is directly determined from the properties of the FRCM fibers without the need for the estimation of debonding strains and experimental results of the FRCM composite. The collected database is normalized into a [0, 1] range to overcome the problems related to the low learning rates of ML models at the extreme values of the parameters.

4.1. Single AI models

4.1.1. Kernel ridge regression

Kernel ridge regression (KRR) is a nonlinear regression that maps data into different dimensional spaces ($x_i \rightarrow \Phi_i = \Phi(x_i)$) using kernel trick. It addresses the limitations of the well-known least square (LS) method using ridge regression (linear least squares with I2-norm regularization) and kernel function. Thus, it extends the ridge regression to include nonlinear problems using a nonlinear map. For nonlinear regression, KRR transforms the nonlinear regression in the original space into a linear regression in a higher dimensional space using a nonlinear kernel function. The widely used kernels include linear, polynomial, hyperbolic tangent (sigmoid), and radial basis function (RBF) kernels [78].

The KRR can be formulated as [79]:

$$y = K\alpha + \varepsilon \tag{11}$$

where ε is the error vector and α is the KRR unknown vector determined by minimizing Eq. (12).

$$f(\alpha) = 0.5(y - K\alpha)^T(y - K\alpha) + 0.5\lambda\alpha^T K\alpha, \lambda \geq 0 \tag{12}$$

where λ is the regularization parameter.

The solution with respect to α can be given by [79]:

$$\alpha = (K + \lambda I_n)^{-1} y \tag{13}$$

The KRR solution in Eq. (13) can be rewritten as:

$$y = (K + \lambda I_n)\alpha \tag{14}$$

The kernel type and parameters α and λ are optimized to find the best model.

4.1.2. K-nearest neighbors

The K-nearest neighbors (KNN) is a non-parametric model that can be used for classification as well as regression problems. The KNN regression approximates the relationship between the input features and target variable using the observations of K nearest neighbors. To make a prediction for a query point, the algorithm firstly measures the distance between the training data points and the query data point using Euclidean distance and orders the calculated distance in ascending order. The algorithm then identifies the K training data points closest to the query data point, represented by N_0. Finally, the target value for the query data point is estimated as the weighted mean of all the training responses in N_0. The size of the neighborhood K needs to be optimized.

4.1.3. Support vector regression

Support vector regression (SVR) uses a mapping procedure to map the input to a high-dimensional feature space. Given n number of training examples $\{(x_i, y_i)\}_{i=1}^{n} \in \mathbb{R}^n \times \mathbb{R}$, SVR estimates the regression function $f(x)$ in Eq. (15) by minimizing the regularized risk function in Eq. (15a) subject to Eqs. (15b) and (15c) [80].

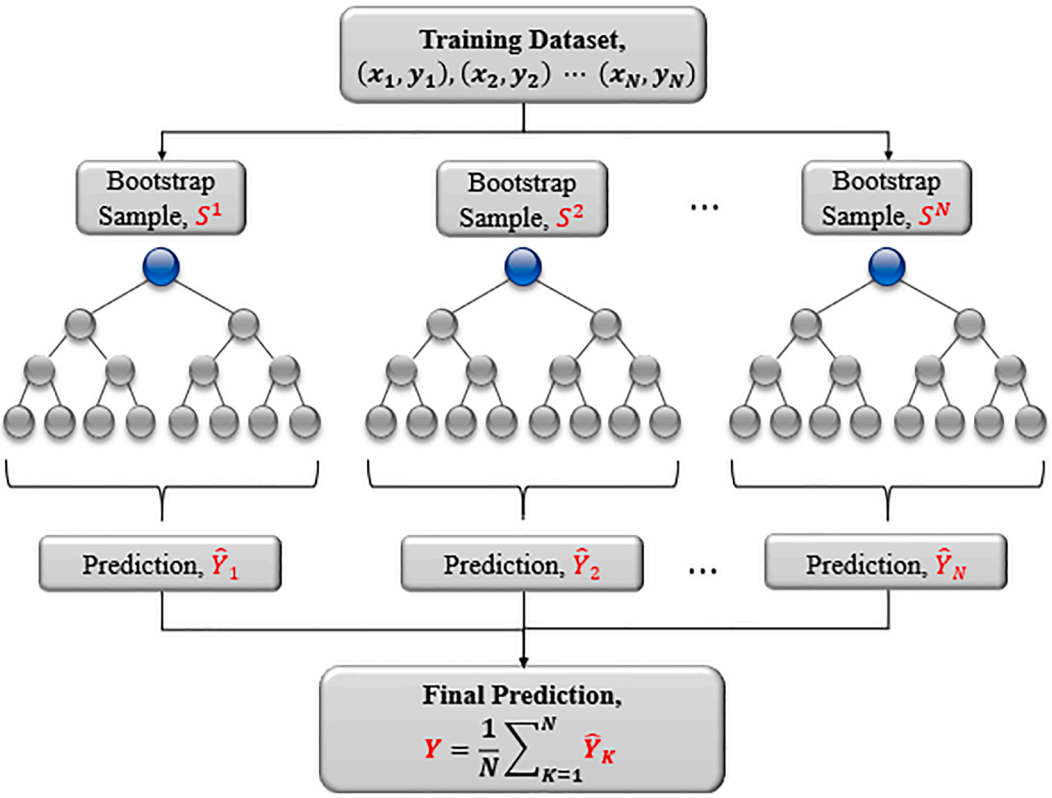

Fig. 4. Learning process of random forest algorithm.

$$f(x) = w.\phi(x) + b \tag{15}$$

$$\tau(w, \xi, \xi^*) = \frac{1}{2}\|w\|^2 + C\frac{1}{n}\sum_{i=1}^{n}(\xi_i + \xi_i^*), i = 1, 2, \cdots, n \tag{15a}$$

$$(w.\phi(x) + b) - y_i \leq \varepsilon + \xi_i, i = 1, 2, \cdots, n \tag{15b}$$

$$y_i - (w.\phi(x) + b) \leq \varepsilon + \xi_i^*, i = 1, 2, \cdots, n \tag{15c}$$

$$x_i \epsilon X \subseteq R^n, y_i \epsilon Y \subseteq R \tag{15d}$$

$$\xi_i, \xi_i^* \geq 0 \tag{15e}$$

where,

ξ_i and ξ_i^* are slack variables,
w and b are weight vector and the bias, estimated by minimizing Eq. (15a) subject to Eqs. (15b) and (15c) [80],
ε is Vapnik's insensitive loss that serves as a threshold, in which the absolute values of errors less than ε are ignored, and
C is a regularization parameter.

The prediction in SVR is given by [78,81]:

$$f(x) = \sum_{i \epsilon SV}(\alpha_i - \alpha_i^*)K(x_i, x) + b \ \ subject\ to\ 0 \leq \alpha_i \leq C,\ 0 \leq \alpha_i^* \leq C \tag{16}$$

where $K(x_i, x)$ is the kernel function, α_i and α_i^* are the Lagrange multipliers, and SV denotes support vectors, which are subsets of training data.

4.1.4. Decision trees

Decision trees also known as classification and regression trees or CART for short is a non-parametric rule-based algorithm that can be used for classification as well as regression problems using a simple tree structure [82]. In CART, the feature space is partitioned into several smaller disjoint regions with similar response values using a set of splitting rules utilizing tree-like structures. Each internal node in CART specifies a test on an attribute of the data, while each branch represents the test output. The root node in CART represents the most relevant feature. Given training examples $\{(x_i, y_i)\}_{i=1}^{n}$, where $x_i \epsilon X$ and $y_i \epsilon Y$, decision tree regression recursively partitions the input feature space into disjoint regions R_k assigned to each leaf of the CART and estimate the response within each region.

A single decision tree model is associated with the problem of overfitting and possesses high variance. To mitigate or reduce this problem, different ensemble models are used, as will be discussed below.

4.2. Ensemble models

Ensemble learners integrate several base learners to enhance the generalization ability over a single model [82]. Bagging and boosting ensembles are widely used techniques for improving prediction performance. They are commonly applied to tree-based learners although they can be applied to other learners also such as artificial neural networks [82]. The basic idea behind the ensemble model is to combine multiple base learners in computing the final response rather than relying on an individual model.

4.2.1. Random forest

Random forest (RF) is a combination of multiple randomly created decision tree predictors. Each decision tree predictor in the random forest algorithm uses bootstrap samples, which are randomly selected samples from the original training dataset with replacement. Moreover, random subsets of input features are considered when splitting nodes in the decision tree on the best split among a random subset of the features selected at every node [83]. The split at each node is performed in two steps. Firstly, a random subset of input features is selected from the bootstrap sample [83]. The best subset feature is then selected to

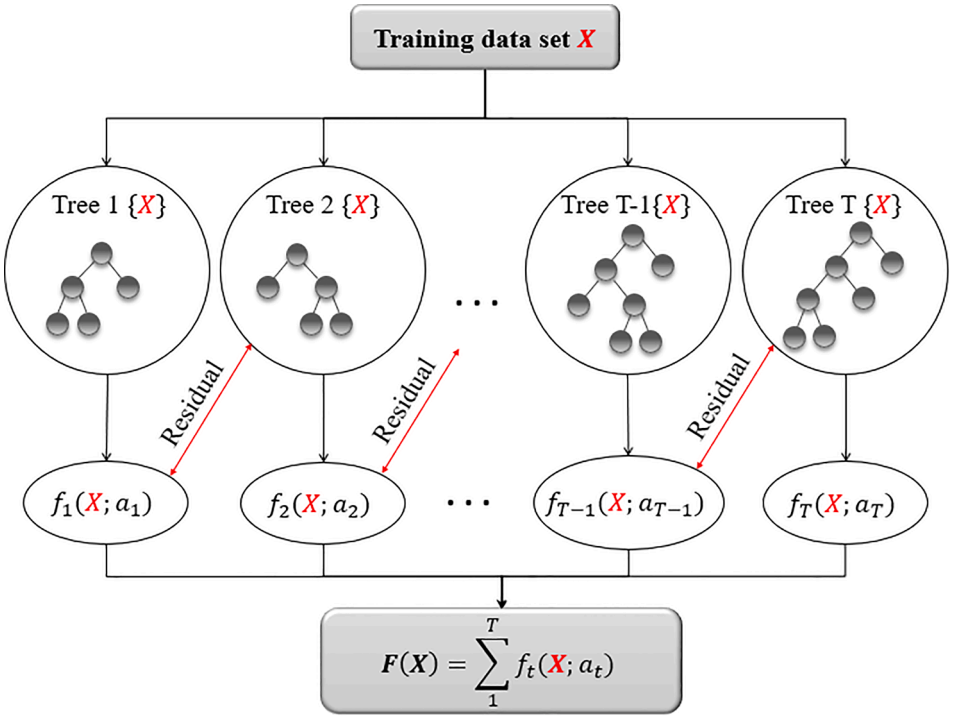

Fig. 5. Schematic of boosting algorithm.

perform the decision split at each node of a decision tree [83]. Fig. 4 shows a simple schematic of the RF algorithm. The final prediction of RF is made by averaging the predictions of each decision tree predictor, as shown in Fig. 4.

4.2.2. Gradient boosted trees

Gradient boosted trees (GBT) is one of the powerful boosting algorithms, which combines a sequence of weak learners; particularly classification and regression trees in an additive model. Fig. 5 illustrates the learning process in the boosting algorithm. The GBT is mathematically expressed as follows:

$$F_T(x) = \sum_{t=0}^{T} f_t(x) \tag{17}$$

where T is the number of base learners (CARTs) and f_t is the set of all possible decision trees.

Given a training dataset $\{(x_1, y_1), (x_2, y_2), \cdots, (x_n, y_n)\}$ with n observations and a differentiable loss function $L(y_i, F(x))$, gradient boosted trees performs the following steps [84]:

(1) Initialize the model with a constant value that minimizes the loss:

$$F_0(x) = \underset{\rho}{argmin} \sum_{i=1}^{n} L(y_i, \rho) \tag{18}$$

(2) For $t = 1$ to T do:

a. Determine the negative gradient of the loss or pseudo residuals, given the previous ensemble F_{t-1}:

$$r_{it} = -\frac{\partial L[y_i, F_{t-1}(x_i)]}{\partial F_{t-1}(x_i)} \tag{19}$$

b. Fit CART to r_{it} values and create terminal regions R_{jt}, *for* $j = 1, 2, \cdots, j_t$, where j_t is the number of terminal nodes.

c. For $j = 1, 2, \cdots, j_t$ compute the output value for each leaf that minimizes the loss:

$$\rho_{jt} = \underset{\rho}{argmin} \sum_{x_i \in R_{ij}} L(y_i, F_{t-1}(x_i) + \rho) \tag{20}$$

d. Update the estimator of $F(x)$:

$$F_t(x) = F_{t-1}(x) + v \sum_{j=1}^{j_t} \rho_{jt} I_{x \in R_{jt}}(x) \tag{21}$$

where v is the learning rate [84].

(3) Output $F_T(x)$.

4.2.3. Extreme gradient boosting

The extreme gradient boosting (xgBoost) algorithm developed by Chen and Guestrin [85] is an improved form of gradient boosting algorithm. The xgBoost adds a regularization term in the objective function in order to reduce model complexity and prevent overfitting. The base learners (trees) in the xgBoost are built sequentially by minimizing the objective function [85] in Eq. (22), which contains the loss function and regularization term:

$$\sum_{i=1}^{n} L(y_i, \widehat{y_i}) + \sum_{t=1}^{T} \Omega(f_t) \tag{22}$$

$$\Omega(f) = \gamma T + \frac{1}{2} \lambda \sum_{j=1}^{T} w_j^2 \tag{23}$$

where γ is the complexity of each leaf, w_j is the weight of leaf j, and λ is the penalty parameter.

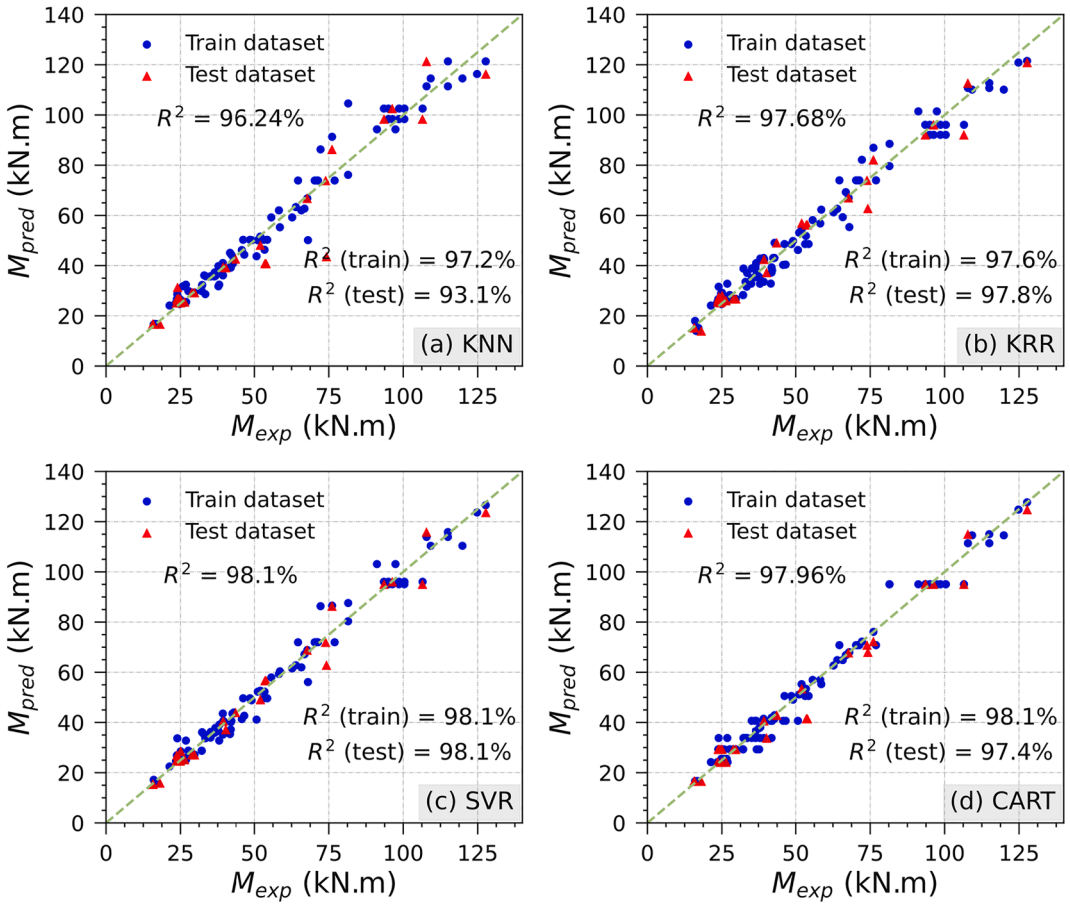

Fig. 6. Experimental versus predicted flexural capacities of FRCM-strengthened beams based on single models.

5. Hyperparameter tuning and cross-validation

The values of hyperparameters of a given model determine the predictive performance and generalization capability of the model. The optimal values of the hyperparameters are chosen with the help of hyperparameter tuning or optimization. Grid search is a widely used hyperparameter tuning technique. To prevent over-fitting problems, a *K*-fold cross-validation method is adopted during the hyperparameter tuning process. Firstly, the dataset is split into training and testing datasets comprised of 80% and 20% of the completed dataset, respectively. The *K*-fold cross-validation is then performed based on the following three steps:

(a) Partition the training dataset into independent *K*-groups or folds of equal size without replacement so that each observation will be used for training and validation exactly once.
(b) Fit the model using $K-1$ folds and validate the model based on the remaining one fold, and
(c) Repeat step (b) *K* times so that *K* number of performance indices are obtained.

The final performance of the model is taken as the mean of *K* performance indices. In this study, a 10-fold cross-validation ($K = 10$) is combined with a grid search algorithm to optimize the hyperparameters. In 10-fold cross-validation, 10% of the training dataset is used as a validation dataset in each iteration, while the remaining 90% of the training dataset is used to train the model.

6. Results and discussion

In this section, the prediction capability of the developed ML models is investigated. The performance of the models is assessed using different performance indices including mean absolute error (MAE), mean absolute percentage error (MAPE), root mean squared error (RMSE), and coefficient of determination (R^2). Moreover, the comparison of the existing models with the developed ML models is presented herein. The performance indices are presented mathematically by Eqs. (24a)–(24d).

$$MAE = \frac{1}{N}\sum_{i=1}^{N}|y_i - \hat{y}_i| \tag{24a}$$

$$MAPE = \frac{1}{N}\sum_{i=1}^{N}\left|\frac{y_i - \hat{y}_i}{y_i}\right| \tag{24b}$$

$$RMSE = \sqrt{\frac{1}{N}\sum_{i=1}^{N}(y_i - \hat{y}_i)^2} \tag{24c}$$

$$R^2 = 1 - \frac{\sum_{i=1}^{N}(y_i - \hat{y}_i)^2}{\sum_{i=1}^{N}(y_i - \bar{y})^2} \tag{24d}$$

where y and $\hat{y}$ are the target and predicted values, respectively, $\bar{y}$ is the mean of y values, and N is the number of data points.

6.1. Model prediction results

Fig. 6a–d show the scatter plots for the predicted (M_{pred}) versus experimental (M_{exp}) flexural capacities using the single ML models, while Fig. 7a–c compare the experimental and predicted flexural

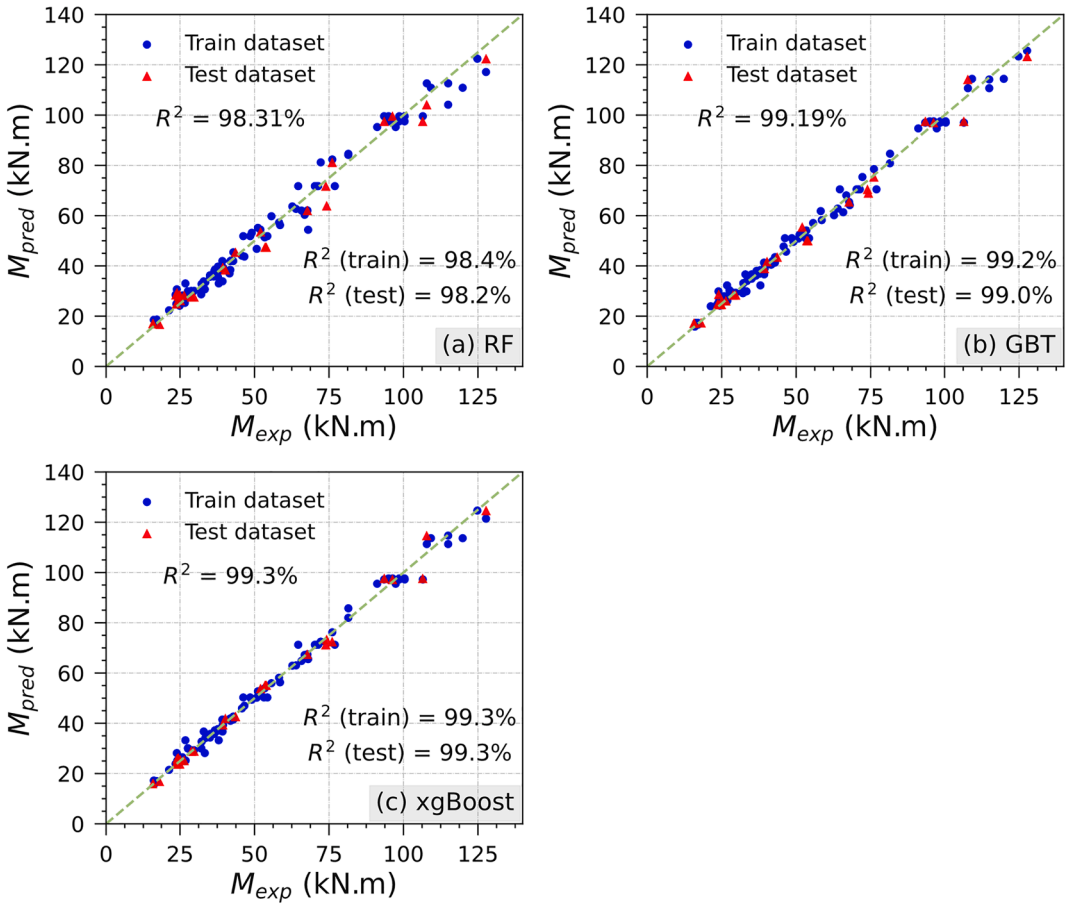

Fig. 7. Experimental versus predicted flexural capacities of FRCM-strengthened beams based on ensemble models.

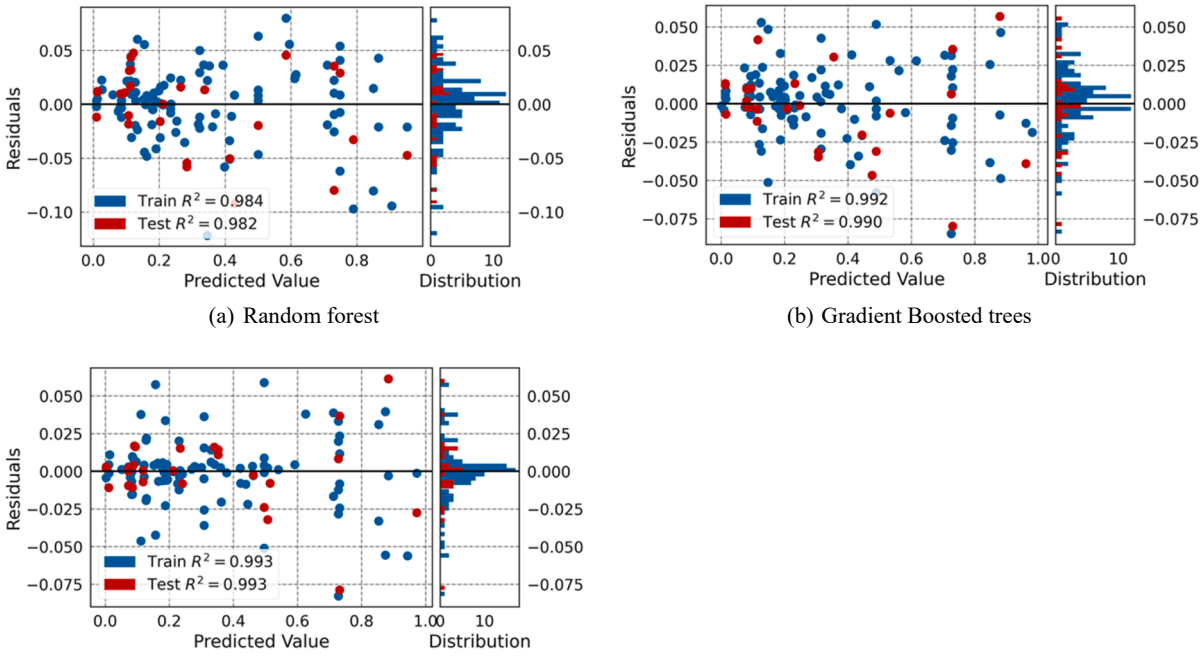

(a) Random forest

(b) Gradient Boosted trees

(c) xgBoost

Fig. 8. Residual of the predicted load capacity on the normalized training and test datasets for ensemble models.

Table 2
Performance indices of different ML models.

Model	Training dataset				Test dataset			
	RMSE (kN·m)	MAE (kN·m)	MAPE (%)	R^2 (%)	RMSE (kN·m)	MAE (kN·m)	MAPE (%)	R^2 (%)
KNN	4.80	3.10	5.87	97.2	8.43	5.15	9.30	93.1
KRR	4.45	3.56	7.86	97.6	4.71	3.37	7.32	97.8
SVR	3.97	2.72	5.77	98.1	4.44	3.04	6.01	98.1
CART	3.95	2.58	5.86	98.1	5.14	3.68	8.44	97.4
RF	3.71	2.67	5.52	98.4	4.30	3.51	7.92	98.2
GBT	2.52	1.84	3.91	99.2	3.19	2.33	4.73	99.0
xgBoost	2.41	1.55	3.17	99.3	2.70	1.77	3.25	99.3

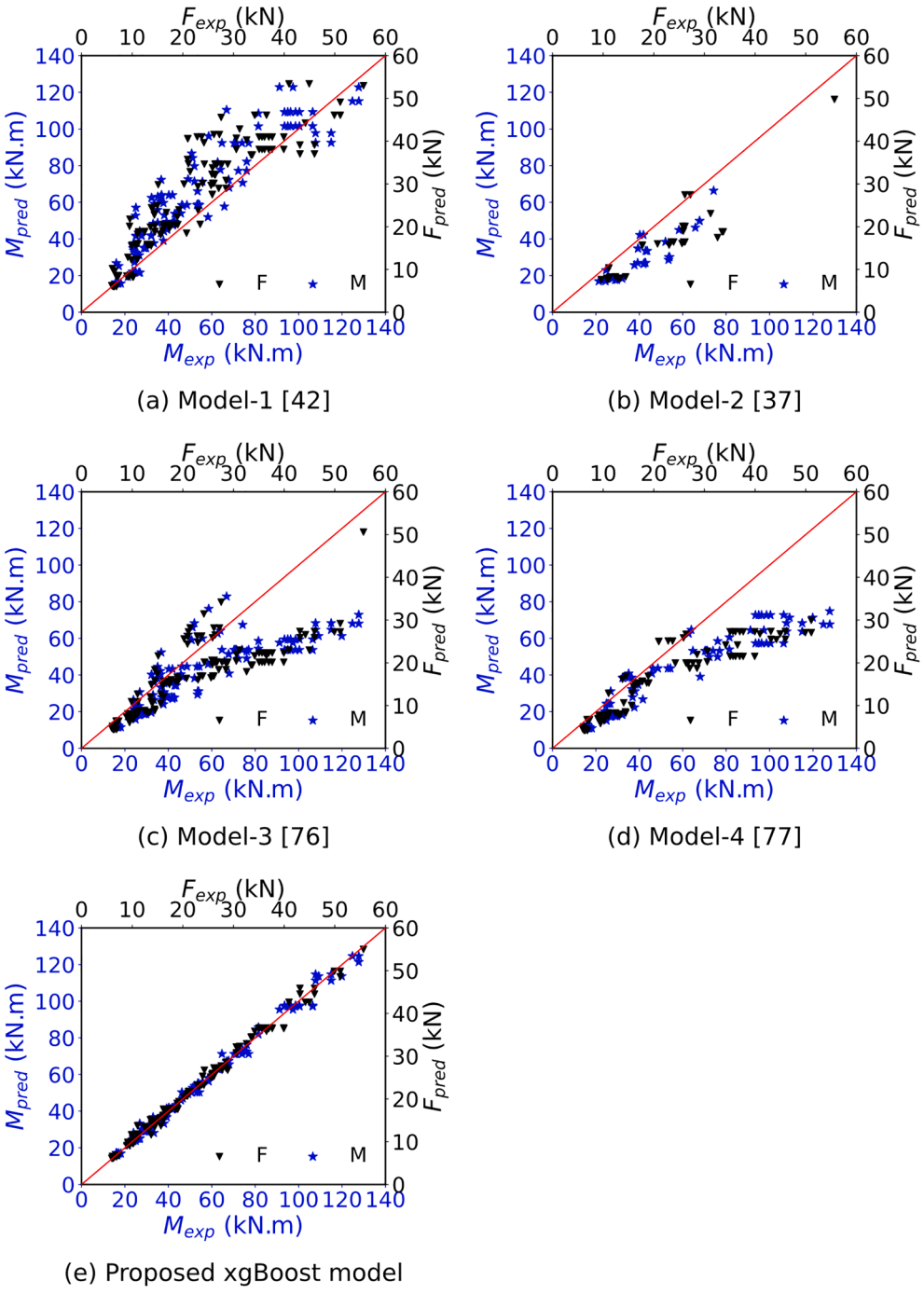

Fig. 9. Experimental versus predicted load capacity of FRCM-strengthened beams based on the existing models.

Table 3
Evaluation of existing and proposed models based on M_{pred}/M_{exp} ratio.

Model	Mean	STD	COV
Model-1 [42]	1.257	0.286	0.228
Model-2 [37]	0.738	0.134	0.182
Model-3 [76]	0.755	0.205	0.272
Model-4 [77]	0.799	0.162	0.203
Proposed xgBoost	1.002	0.048	0.048

STD: Standard deviation; COV: Coefficient of variation.

capacities of the strengthened beams based on the ensemble ML models. Generally, all developed ML models showed a good correlation between the experimental and predicted flexural capacities with $R^2 \geq 93.1\%$. Among the single models, KNN showed the least predictive performance on both the training and test sets, while SVR showed the highest predictive performance, as can be observed in Fig. 6a–d.

For all the ensemble models, as illustrated in Fig. 7a–c, the predicted flexural capacities are well concentrated closely around the 45-degree diagonal line that represents a perfect match between the predicted flexural capacities and the corresponding experimental values. This can

Fig. 10. Explanation of flexural capacity of RC beam strengthened with FRCM in flexure for Specimen CC1 strengthened with PBO-FRCM in [6].

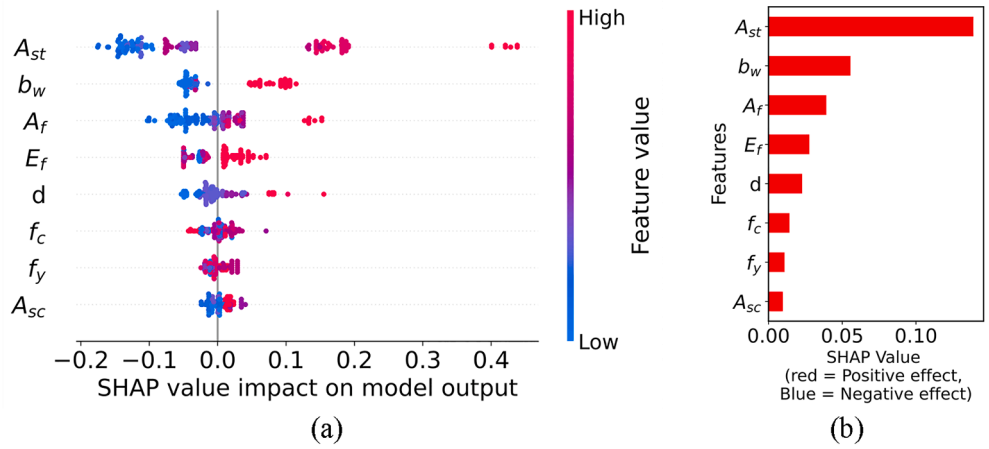

Fig. 11. Summary plot for elucidating the global feature influences of the input features (the color represents the value of the factor varying from low (blue) to high (red)) (a) and global importance of the input features (b).

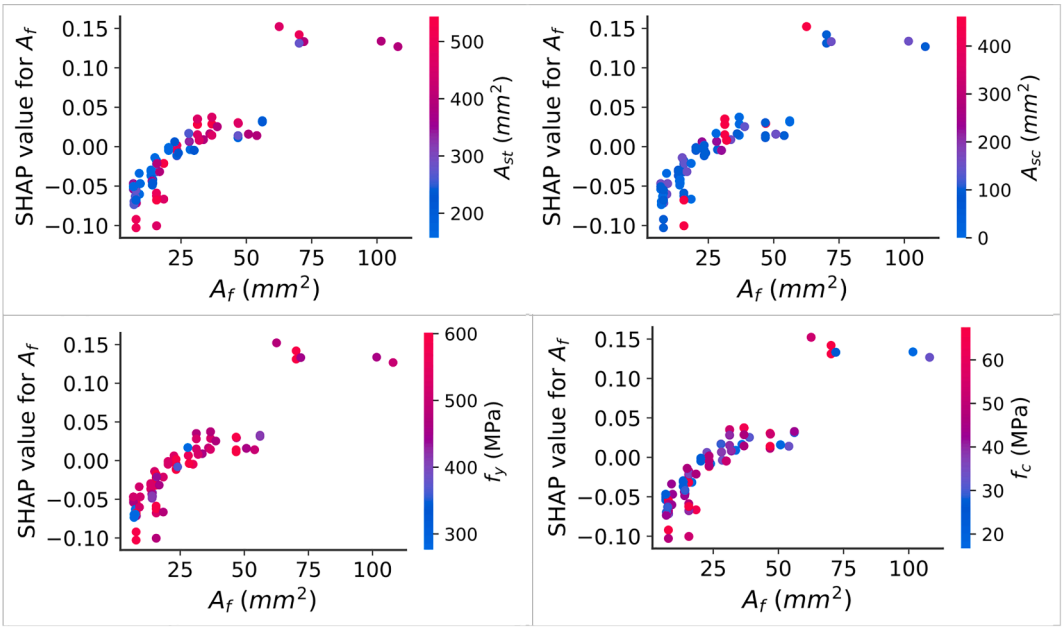

Fig. 12. SHAP dependency and interaction plots.

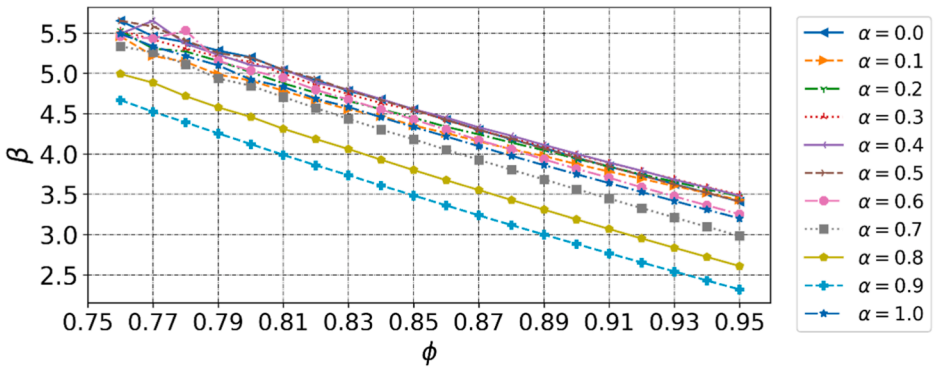

(a) α versus β response

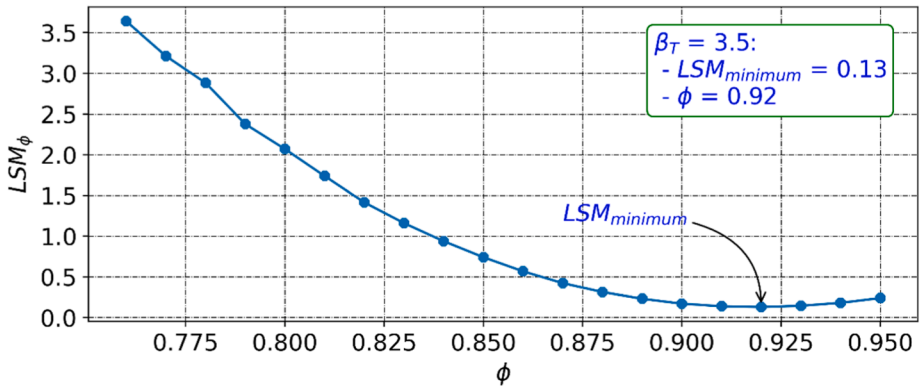

(b) calibration of the strengthe reduction factor

Fig. 13. Reliability index and calibration of strength reduction factor for the proposed xgBoost model.

also be observed in Fig. 8a–c that show the residual of the predicted flexural capacity of the beams, which is the difference between M_{exp} and M_{pred} on the normalized training and test datasets. The figures also provide the coefficient of determination for both the training and test datasets. The residuals for all ensemble models are distributed around zero, as can be seen in Fig. 8a–c. In addition, the proposed ensemble models resulted in a strong correlation between the predicted and experimental flexural capacities as can be evidenced from the values of coefficient of determination, $R^2 \geq 98.2\%$, as can be seen in Fig. 7a–c and Fig. 8a–c. This observation showed that the proposed ensemble models are effective in predicting the flexural capacity of FRCM-strengthened RC beams.

The performance metrics discussed earlier are computed and listed in Table 2 for all models. The results in Table 2 suggested that the predictive performance of all ensemble models is higher than that of the single models (KRR, KNN, SVR, and CART). The CART and SVR models showed a comparable prediction performance on the training set, while the latter performed better on the test set, as listed in Table 2. The KNN resulted in the lowest coefficient of determination (97.2% and 93.1% on the train and test sets, respectively) and the highest RMSE (4.80 kN and 8.43 kN on the train and test sets, respectively), as listed in Table 2.

Among the investigated ML models, the xgBoost model outperformed all other models on both the train and test sets as suggested by the performance metrics in Table 2. The statistical metrics for the xgBoost model are 99.3% (R^2), 2.70 kN·m (RMSE), 1.77 kN·m (MAE), and 3.25% (MAPE) on the test set, as listed in Table 2. The value of the coefficient of determination for the GBT, RF, CART, SVR, KRR, and KNN models was 99.0%, 98.2%, 97.4%, 98.1%, 97.8%, and 93.1%, respectively, compared to R^2 value of 99.3% for the xgBoost model on the test set, as presented in Table 2. Among the ensemble models, the RF model showed the least performance on both the train and test sets. The following section compares the performance of the proposed xgBoost model with that of the existing models in predicting the flexural and load capacities of flexural deficient RC beam strengthened with FRCM.

6.2. Comparison of the proposed and existing models

The predictive performance of the proposed model; particularly, the xgBoost model and the existing models for the FRCM-strengthened RC beams are compared herein. A total of four models proposed by Jung et al. [42], Bencardino et al. [37], Ceroni and Salzano [76], and Mandor and El Refai [77] are used for the comparison purpose, as discussed in Section 2. Model-1 [42] is the most general model developed based on the Teng et al. [75], originally proposed for the FRP system. Hence, it is validated against the complete database. Model-2 [37] is developed for steel FRCM; thus, it is applied to RC beams strengthened with steel FRCM only (a total of 30 beams). The ACI 549.4-20 guideline [38] is based on the elastic modulus and strains in FRCM composites obtained from the test results of FRCM coupons; however, these values are not reported in the majority of the specimens included in the database. Thus, this model [38] is excluded from the comparative study.

Fig. 9a–e illustrate the experimental versus predicted flexural and load capacities based on the existing models [37–42] and the proposed xgBoost. The flexural capacity of the strengthened beams is determined using the existing and proposed models, while the load capacity is determined based on the loading and boundary conditions of the beams. The equity solid line in these figures represents the perfect match between the experimental and predicted responses. Besides, Table 3 presents the evaluation of the existing and proposed models in terms of the average, standard deviation (STD), and coefficient of variation (COV) of

M_{pred}/M_{exp} ratio. Among the existing models, Model-4 [77] showed the best predictive performance with an average of M_{pred}/M_{exp} ratio of 0.799 ± 0.162 and COV of 0.203, as listed in Table 3. As discussed earlier, Model-2 [37] was applied to only 30 specimens strengthened with steel FRCM in the collected database. The average of M_{pred}/M_{exp} ratio based on Model-2 [37] was 0.738 ± 0.134 with COV of 0.182. As can be observed in Fig. 9a–d and Table 3, Model-1 [42] tends to highly overestimate the flexural capacity of the strengthened beams with an average of M_{pred}/M_{exp} ratio of 1.257 ± 0.286 and COV of 0.228. The proposed model showed superior prediction ability compared to the existing models, as can be seen in Fig. 9a–e and Table 3.

6.3. Model explainability using SHAP approach

This study employs the unified SHAP method to explain the outputs of the xgBoost model and highlight the most significant factors and their interactions in determining the flexural capacity of FRCM-strengthened RC beams in flexure. In this approach, the SHAP value, which is the average marginal contribution of each factor is assigned to each factor. The factor with the largest absolute SHAP value is deemed most significant. A typical single prediction plot using the xgBoost model is shown in Fig. 10 (in a natural logarithmic scale), in which the base value denotes the average of the observed response values ($\frac{1}{325}\sum_{i=1}^{325}\ln M_{exp}$). The length and color of the bar in Fig. 10 show the degree of significance and direction (negative or positive) of the effect of each factor, respectively. As can be observed in Fig. 10, the internal tensile reinforcement area (A_{st}) showed the highest effect followed by FRCM reinforcement area and width of the beam section. All factors in Fig. 10 showed positive influences; thus, contributing to the increase in the base value.

The distribution of the Shapley values for each factor across the entire dataset is shown in Fig. 11a. In this figure, each point represents a Shapley value for a feature and an individual observation in the dataset. The position of each dot on the *x*-axis represents a Shapley value for each factor, which shows the influence of each factor on the flexural capacity of the strengthened beams, while the y-axis provides the factors in their order of importance. The color in Fig. 11a shows the value of the factors. For instance, the high value of the internal steel reinforcement area and FRCM area increase the predicted flexural capacity of the strengthened beams.

The global significance of the factors is determined as the average of the absolute Shapley values across the entire dataset (in Fig. 11a) for each factor and plotted in descending order of their importance in Fig. 11b. As can be observed in this figure, the four most influential features are the area of the internal tensile steel reinforcement (A_{st}), width of the beam section (b_w), area of FRCM system, and effective depth of the beam section. On the contrary, A_{sc} is the least influential feature compared to all other factors for the flexural capacity prediction using the proposed xgBoost model. Moreover, the direction of the effect of each factor is shown in the same figure. All factors showed positive effects on the flexural capacity of the strengthened beams, as shown in Fig. 11b. Furthermore, Fig. 12 shows the effect of the internal/external reinforcement interaction on the flexural capacity of the strengthened beams based on the results of SHAP feature dependence analysis. As can be observed in Fig. 12, a negative interaction is observed between the internal/external flexural reinforcements.

7. Reliability analysis of flexural strengthened RC beams with FRCM

Reliability analysis in structural engineering is used to assess the functionality and performance of a structure. To ensure their safety, structures are designed in such a way that their capacity (R) exceeds the demand (Q). According to the load and resistance factor design (LRFD), the limit state in the resistance factor format is given by:

$$\phi R_n \geq \sum \gamma_i Q_i \tag{25}$$

where R_n is the nominal resistance, ϕ is the capacity reduction factor, Q_i is the load effect due to different types of loads (e.g., live load, dead load, snow load, etc.), and γ_i is the load partial safety factor. Considering the effect of only the dead load (P_{DL}) and live load (P_{LL}), according to ACI 318 [86], the limit state in Eq. (25) can be given by:

$$\phi R_n \geq 1.4P_{DL} \tag{26a}$$

$$\phi R_n \geq 1.2P_{DL} + 1.6P_{LL} \tag{26b}$$

The selection of the target reliability index depends on the consequences of failure [87]. According to [87], the target reliability index is taken between 3.0 and 3.5 for flexural members. In this paper, the reduction factor is calibrated for the flexural capacity of RC beams strengthened in flexure with FRCM based on the proposed xgBoost model to achieve a target reliability index of 3.5. The reliability index (β) can be defined as follows, in terms of the probability of failure (P_F):

$$\beta = \varphi^{-1}(1 - P_F) \tag{27}$$

where φ^{-1} is the inverse of standard normal cumulative distribution.

According to Szerszen and Nowak [88], a normal distribution is assumed for both dead load and live load distributions. The bias and coefficient of variation of the dead load for cast-in-situ concrete are taken as 1.05 and 0.1, respectively [88]. The statistical parameters for a 50-year live load are taken as 1.0 (bias) and 0.18 (COV). The distribution parameters for the capacity R are determined based on the collected experimental database. The determination of the reliability index in this study can be summarized as follows:

- Assuming dead load to total load ratios ($\alpha = P_{DL}/(P_{DL} + P_{LL})$) of $\alpha = 0.0 : 0.1 : 1.0$, generate a total of 250 million simulations for each α using the Monte Carlo Simulation.
- Determine the nominal capacity of the beam based on the governing limit state in Eqs. (26a) and (26b). The actual mean is the product of the nominal mean and bias.
- Determine the reliability index based on Eq. (27). The probability of failure corresponds to the probability of $R < Q$.
- Calibrate the resistance reduction factor to achieve a target reliability index (β_T) of 3.50 using the least square method in Eq. (28).

$$LSM = \frac{1}{n}\sum_{i=1}^{n}(\beta_i - \beta_T)^2 \tag{28}$$

where *LSM* is the least square mean and β_i is the reliability at a particular ϕ.

A range of capacity reduction factor $\phi = 0.750 : 0.01 : 0.95$ was analyzed and the value of β corresponding to each ϕ was determined and results are plotted in Fig. 13a. As expected, the value of β increased with a decrease in ϕ, as shown in Fig. 13a. The larger safety margin corresponds to a smaller value of the resistance reduction factor. Fig. 13b shows the variation of *LSM* with the change in ϕ for a target reliability index of 3.5. As shown in this figure, the minimum *LSM* corresponds to a capacity reduction factor of 0.92. Hence, a reduction factor of 0.92 is recommended to achieve a target reliability index of 3.5 for RC beams strengthened in flexure with FRCM based on the proposed xgBoost model. A design example is provided in Appendix A to illustrate the design of the FRCM system for flexural strengthening of RC beams based on the calibrated ϕ using the proposed xgBoost model.

8. Conclusions

A substantial amount of research efforts has been devoted to experimentally investigate the flexural behavior of FRCM-strengthened RC beams; however, the available analytical studies are limited. Moreover,

there exists a large discrepancy in the predictions of the flexural and load capacities of FRCM-strengthened RC beams using the existing models. Therefore, it is crucial to enrich the literature with a more accurate and reliable model. To this end, this paper applies different machine learning models to predict the flexural and load capacities of flexural strengthened RC beams using different types of FRCM systems (carbon FRCM, PBO FRCM, and steel FRCM) for the first time. A total of nine input parameters that describe the beam geometry, mechanical characteristics of materials, and reinforcement area of steel bars and FRCM are included in the database. The predictive performance of the existing models is also presented and compared with that of the proposed model. The use of a unified SHAP method is investigated to explain the predicted response and rank the input features and their interactions for the flexural capacity of FRCM-strengthened beams based on the proposed xgBoost model. Finally, a reliability analysis is performed to calibrate a resistance reduction factor to achieve a target reliability index of 3.50 based on the proposed xgBoost model. The following conclusions can be drawn from this study:

- Among the existing models, Model-4 [77] resulted in the most accurate predictions with an average of M_{pred}/M_{exp} ratio of 0.799 ± 0.162 and COV of 0.203. Model-1 [42], which was developed based on Teng et al. [75] model for the FRP system, provided unsafe predictions for most of the strengthened beams with an average of M_{pred}/M_{exp} ratio of 1.257 ± 0.286 and COV of 0.228.
- Generally, all the developed ML models showed good prediction accuracy. The xgBoost model achieved the best predictive ability with the least RMSE, MAE, and MAPE values and the highest R^2 on both the training and test datasets. The value of R^2 using the xgBoost model was 99.3% and 99.2% for the training and test datasets, respectively.
- A comparative study between the proposed and existing models revealed the superior predictive capability and robustness of the proposed model. The predicted flexural and load capacities of the strengthened beams based on the existing models are highly scattered and unsafe.
- Based on the results of SHAP, it is noted that the area of internal tensile steel reinforcement, area of FRCM reinforcement, and width and depth of the beam section have the most significant influences on the flexural capacity of the strengthened beams.
- A capacity reduction factor $\phi = 0.92$ is calibrated to achieve a reliability index $\beta_T = 3.5$. A design example is provided in Appendix A to illustrate the design of the FRCM strengthening system for flexural deficient RC beams based on the proposed xgBoost model and calibrated reduction factor.

The present study can contribute to the state-of-the-art for design and flexural strengthening of RC beams. However, the results of this study are limited to the parameters investigated. Therefore, future research is recommended to investigate the application of data-driven ML models to predict the failure mode of RC beams strengthened in flexure and capacity and failure mode of RC beams strengthened in shear.

9. Data availability statement

Some or all data, models, or codes that support the findings of this study are available from the corresponding author upon reasonable request.

CRediT authorship contribution statement

Tadesse G. Wakjira: Conceptualization, Formal analysis, Investigation, Methodology, Visualization, Software, Writing – original draft, Writing – review & editing. **Mohamed Ibrahim:** Conceptualization, Formal analysis, Investigation, Methodology, Visualization, Writing – original draft, Writing – review & editing. **Usama Ebead:** Conceptualization, Supervision, Validation, Writing – review & editing. **M. Shahria Alam:** Conceptualization, Supervision, Validation, Writing – review & editing.

Declaration of Competing Interest

The authors declare that they have no known competing financial interests or personal relationships that could have appeared to influence the work reported in this paper.

Acknowledgment

This paper was made possible by NPRP grant # NPRP 13S-0209-200311 from the Qatar National Research Fund (a member of Qatar Foundation) and financial support of the Natural Sciences and Engineering Research Council (NSERC) of Canada. Open Access funding provided by the Qatar National Library. The findings achieved herein are solely the responsibility of the authors.

Appendix A. Design example

A simply supported RC bridge beam is seriously damaged due to corrosion on its bottom face (Fig. A1). The beam is estimated to have lost 20% of its flexural reinforcement due to corrosion. Design the required FRCM reinforcement for strengthening of the beam and recovering its flexural capacity.

Details of the existing beam:

- Cross-sectional dimensions: 200 × 250 mm ($b_w \times d$).
- Concrete strength: $f_c = 30$ MPa,
- Yield strength of steel bars: $f_y = 420$ MPa,
- Longitudinal tension reinforcement: 4 bars with 14 mm diameter, and
- Longitudinal compression reinforcement: 2 bars with 14 mm diameter.

Flexural capacity of the beam before strengthening:

- Nominal flexural capacity before damage: $M_n = 58.1$ kN·m
- Nominal flexural capacity after damage: $M_{nd} = 46.48$ kN·m

Try two layers of carbon FRCM:
Selected FRCM fabrics: bi-directional carbon fabrics (Fig. A2) with the following properties:

- Grid spacing: 10 × 10 mm,
- Area of fiber per unit width in both the weft and warp directions: 047 mm^2/mm, and
- Elastic modulus: $E_f = 240$ GPa.

Flexural capacity of the strengthened beam:

$A_f = n_f t_f b_f = 18.8\ mm^2, A_{st} = 523.39\ mm^2, A_{sc} = 307.88\ mm^2$

- Determine the nominal flexural capacity using the proposed xgBoost model. A web-based application, which is under development using the proposed xgBoost model is available at https://beamcapacity.herokuapp.com/. The predicted nominal flexural capacity of the strengthened beam ($M_{n,new}$) is determined to be:

$M_{n,new} = 65.75$ kN·m

- Check the flexural capacity of the strengthened beam against that of the original beam before damage:

$M_{n,new} = 65.75\ kN{\cdot}m \geq M_n = 58.1\ kN{\cdot}m, OK$

- Determine the design flexural capacity:

$M_{r,new} = \phi M_{n,new} = 0.92 \times 65.75\ kN{\cdot}m = 60.49\ kN{\cdot}m$

Fig. A1. Schematic of the beam and cross-sectional details.

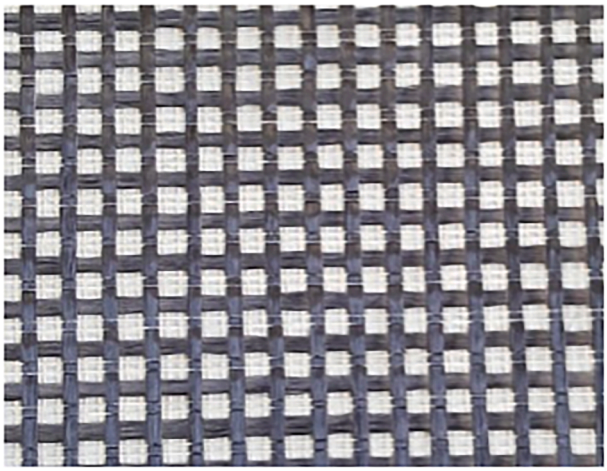

Fig. A2. Selected FRCM fabrics [89].

References

[1] Elsanadedy HM, Abbas H, Almusallam TH, Al-Salloum YA. Organic versus inorganic matrix composites for bond-critical strengthening applications of RC structures – state-of-the-art review. Compos Part B Eng 2019;174:106947. https://doi.org/10.1016/j.compositesb:2019.106947.

[2] Koutas L, Tetta ZC, Bournas D, Triantafillou T. Strengthening of concrete structures with Textile Reinforced Mortars: state-of-the-Art Review. J Compos Constr 2019; 23:03118001. https://doi.org/10.1061/(ASCE)CC.1943-5614.0000882.

[3] Koutas L, Bournas D. Flexural strengthening of two-way RC slabs with textile-reinforced mortar: experimental investigation and design equations. J Compos Constr 2017;21:1–11.

[4] Babaeidarabad S, Loreto G, Nanni A. Flexural strengthening of RC beams with an externally bonded fabric-reinforced cementitious matrix. J Compos Constr 2014; 18:1–12. https://doi.org/10.1061/(ASCE)CC.1943-5614.0000473.

[5] Ombres L. Flexural analysis of reinforced concrete beams strengthened with a cement based high strength composite material. Compos Struct 2011;94(1): 143–55. https://doi.org/10.1016/j.compstruct.2011.07.008.

[6] D'Ambrisi A, Focacci F. Flexural strengthening of RC beams with cement-based composites. J Compos Constr 2011;15(5):707–20. https://doi.org/10.1061/(ASCE)CC.1943-5614.0000218.

[7] Hashemi S, Al-Mahaidi R. Investigation of flexural performance of RC beams strengthened with CFRP textile and cement based adhesives. Proc the 3rd Asia-pacific conference on FRP in structures. 2012.

[8] Barton B, Wobbe E, Dharani LR, Silva P, Birman V, Nanni A, et al. Characterization of reinforced concrete beams strengthened by steel reinforced polymer and grout (SRP and SRG) composites. Mater Sci Eng, A 2005;412(1-2):129–36. https://doi.org/10.1016/j.msea.2005.08.151.

[9] Elsanadedy H, Almusallam T, Alsayed S, Al-Salloum Y. Flexural strengthening of RC beams using textile reinforced mortar – experimental and numerical study. Compos Struct 2013;97:40–55. https://doi.org/10.1016/j.compstruct.2012.09.053.

[10] Pellegrino C, D'Antino T. Experimental behaviour of existing precast prestressed reinforced concrete elements strengthened with cementitious composites. Compos Part B Eng 2013;55:31–40. https://doi.org/10.1016/j.compositesb.2013.05.053.

[11] Raoof S, Koutas L, Bournas D. Textile-reinforced mortar (TRM) versus fibre-reinforced polymers (FRP) in flexural strengthening of RC beams. Constr Build Mater 2017;151:279–91. https://doi.org/10.1016/j.conbuildmat.2017.05.023.

[12] Elghazy M, El Refai A, Ebead U, Nanni A. Post-repair flexural performance of corrosion-damaged beams rehabilitated with fabric-reinforced cementitious matrix (FRCM). Constr Build Mater 2018;166:732–44. https://doi.org/10.1016/j.conbuildmat.2018.01.128.

[13] Pino V, Akbari Hadad H, De Caso y Basalo F, Nanni A, Ali Ebead U, El Refai A. Performance of FRCM-strengthened RC beams subject to fatigue. J Bridg Eng 2017;22(10):04017079. https://doi.org/10.1061/(ASCE)BE.1943-5592.0001107.

[14] Triantafillou TC. Innovative textile-based composites for strengthening and seismic retrofitting of concrete and masonry structures. In: Proc the 5th international conference on FRP composites in civil engineering, CICE-2010, Beijing China; 2010.

[15] Menna C, Asprone D, Ferone C, Colangelo F, Balsamo A, Prota A, et al. Use of geopolymers for composite external reinforcement of RC members. Compos Part B Eng 2013;45(1):1667–76.

[16] Escrig C, Gil L, Bernat-Maso E. Experimental comparison of reinforced concrete beams strengthened against bending with different types of cementitious-matrix composite materials. Constr Build Mater 2017;137:317–29.

[17] Ombres L. Failure modes in reinforced concrete beams strengthened with PBO fiber reinforced mortars. In: Proc, fiber-reinforced polymer reinforcement for concrete structures, FRPRCS-9, Sydney, Australia; 2009.

[18] Elghazy M, El Refai A, Ebead U, Nanni A. Corrosion-damaged RC beams repaired with fabric-reinforced cementitious matrix. J Compos Constr 2018;22(5):04018039. https://doi.org/10.1061/(ASCE)CC.1943-5614.0000873.

[19] El-Sherif HE, Wakjira TG, Ebead U. Flexural strengthening of reinforced concrete beams using hybrid near-surface embedded/externally bonded fabric-reinforced cementitious matrix. Constr Build Mater 2020;238:117748. https://doi.org/10.1016/j.conbuildmat.2019.117748.

[20] Wakjira TG, Ebead U. Hybrid NSE/EB technique for shear strengthening of reinforced concrete beams using FRCM: experimental study. Constr Build Mater 2018;164:164–77. https://doi.org/10.1016/j.conbuildmat.2017.12.224.

[21] Ebead U, Shrestha KC, Afzal MS, El Refai A, Nanni A. Effectiveness of fabric-reinforced cementitious matrix in strengthening reinforced concrete beams. J Compos Constr 2017;21(2):04016084. https://doi.org/10.1061/(ASCE)CC.1943-5614.0000741.

[22] Ebead U, El Refai A, Shrestha K, Nanni A. Soffit and U-wrap fabric-reinforced cementitious matrix strengthening for reinforced concrete beams. ACI Struct J 2019;116:267–78. https://doi.org/10.14359/51713292.

[23] Loreto G, Leardini L, Arboleda D, Nanni A. Performance of RC slab-type elements strengthened with fabric-reinforced cementitious-matrix composites. J Compos Constr 2013;18:A4013003. https://doi.org/10.1061/(ASCE)CC.1943-5614.0000415.

[24] Hashemi S, Al-Mahaidi R. Experimental and finite element analysis of flexural behavior of FRP-strengthened RC beams using cement-based adhesives. Constr Build Mater 2012;26(1):268–73. https://doi.org/10.1016/j.conbuildmat.2011.06.021.

[25] Sneed L, Verre S, Carloni C, Ombres L. Flexural behavior of RC beams strengthened with steel-FRCM composite. Eng Struct 2016;127:686–99. https://doi.org/10.1016/j.engstruct.2016.09.006.

[26] Bencardino F, Condello A. Structural behaviour of RC beams externally strengthened in flexure with SRG and SRP systems. Int J Struct Eng 2014;5:346–68. https://doi.org/10.1504/IJSTRUCTE.2014.065928.

[27] Napoli A, Realfonzo R. Reinforced concrete beams strengthened with SRP/SRG systems: experimental investigation. Constr Build Mater 2015;93:654–77. https://doi.org/10.1016/j.conbuildmat.2015.06.027.

[28] Bournas D, Lontou PV, Papanicolaou C, Triantafillou T. Textile-reinforced mortar versus fiber-reinforced polymer confinement in reinforced concrete columns. ACI Struct J 2007;104:740–8. https://doi.org/10.14359/18956.

[29] Ombres L, Verre S. Structural behaviour of fabric reinforced cementitious matrix (FRCM) strengthened concrete columns under eccentric loading. Compos Part B Eng 2015;75:235–49.

[30] Cascardi A, Longo F, Micelli F, Aiello MA. Compressive strength of confined column with Fiber Reinforced Mortar (FRM): new design-oriented-models. Constr Build Mater 2017;156:387–401. https://doi.org/10.1016/j.conbuildmat.2017.09.004.

[31] Ombres L. Concrete confinement with a cement based high strength composite material. Compos Struct 2014;109:294–304. https://doi.org/10.1016/j.compstruct.2013.10.037.

[32] Caggegi C, Carozzi FG, De Santis S, Fabbrocino F, Focacci F, Hojdys Ł, et al. Experimental analysis on tensile and bond properties of PBO and aramid fabric reinforced cementitious matrix for strengthening masonry structures. Compos Part B Eng 2017;127:175–95.

[33] D'Ambrisi A, Focacci F, Luciano R, Alecci V, De Stefano M. Carbon-FRCM materials for structural upgrade of masonry arch road bridges. Compos Part B Eng 2015;75:355–66. https://doi.org/10.1016/j.compositesb.2015.01.024.

[34] Carozzi FG, Poggi C. Mechanical properties and debonding strength of Fabric Reinforced Cementitious Matrix (FRCM) systems for masonry strengthening. Compos Part B Eng 2015;70:215–30. https://doi.org/10.1016/j.compositesb.2014.10.056.

[35] Koutas LN, Bournas DA. Out-of-plane strengthening of masonry-infilled RC frames with textile-reinforced Mortar Jackets. J Compos Constr 2019;23(1):04018079. https://doi.org/10.1061/(ASCE)CC.1943-5614.0000911.

[36] Kouris LAS, Triantafillou TC. State-of-the-art on strengthening of masonry structures with textile reinforced mortar (TRM). Constr Build Mater 2018;188:1221–33. https://doi.org/10.1016/j.conbuildmat.2018.08.039.

[37] Bencardino F, Carloni C, Condello A, Focacci F, Napoli A, Realfonzo R. Flexural behaviour of RC members strengthened with FRCM: State-of-the-art and predictive formulas. Compos Part B Eng 2018;148:132–48. https://doi.org/10.1016/j.compositesb.2018.04.051.

[38] ACI Committee 549. ACI 549.4R-20 Guide to design and construction of externally bonded fabric-reinforced cementitious matrix and steel-reinforced grout systems for repair and strengthening of concrete structures; 2020.

[39] Said H, Wu Z. Evaluating and proposing models of predicting IC debonding failure. J Compos Constr 2008;12(3):284–99. https://doi.org/10.1061/(ASCE)1090-0268(2008)12:3(284).

[40] Lu XZ, Teng JG, Ye LP, Jiang JJ. Intermediate crack debonding in FRP-strengthened RC beams: FE analysis and strength model. J Compos Constr 2007;11(2):161–74.

[41] CNR-DT200 R1/2012. Guide for design and construction of externally bonded FRP systems for strengthening existing structures: materials, RC and PC structures, masonry structures; 2006.

[42] Jung K, Hong K, Han S, Park J, Kim J. Prediction of flexural capacity of RC beams strengthened in flexure with FRP fabric and cementitious matrix. Int J Polym Sci 2015;2015:1–11. https://doi.org/10.1155/2015/868541.

[43] Salehi H, Burgueño R. Emerging artificial intelligence methods in structural engineering. Eng Struct 2018;171:170–89. https://doi.org/10.1016/j.engstruct.2018.05.084.

[44] Demir F. Prediction of elastic modulus of normal and high strength concrete by artificial neural networks. Constr Build Mater 2008;22(7):1428–35. https://doi.org/10.1016/j.conbuildmat.2007.04.004.

[45] Perera R, Ruiz A, Manzano C. An evolutionary multiobjective framework for structural damage localization and quantification. Eng Struct 2007;29(10):2540–50. https://doi.org/10.1016/j.engstruct.2007.01.003.

[46] Lee S-C. Prediction of concrete strength using artificial neural networks. Eng Struct 2003;25(7):849–57. https://doi.org/10.1016/S0141-0296(03)00004-X.

[47] Ben Chaabene W, Flah M, Nehdi ML. Machine learning prediction of mechanical properties of concrete: critical review. Constr Build Mater 2020;260:119889. https://doi.org/10.1016/j.conbuildmat.2020.119889.

[48] Trocoli A, Dantas A, Leite MB, Nagahama KDJ. Prediction of compressive strength of concrete containing construction and demolition waste using artificial neural networks. Constr Build Mater 2013;38:717–22. https://doi.org/10.1016/j.conbuildmat.2012.09.026.

[49] Inel M. Modeling ultimate deformation capacity of RC columns using artificial neural networks. Eng Struct 2007;29(3):329–35. https://doi.org/10.1016/j.engstruct.2006.05.001.

[50] Jiang K, Han Q, Bai Y, Du X. Data-driven ultimate conditions prediction and stress-strain model for FRP-confined concrete. Compos Struct 2020;242:112094. https://doi.org/10.1016/j.compstruct.2020.112094.

[51] Naderpour H, Kheyroddin A, Amiri GG. Prediction of FRP-confined compressive strength of concrete using artificial neural networks. Compos Struct 2010;92(12):2817–29. https://doi.org/10.1016/j.compstruct.2010.04.008.

[52] Jalal M, Ramezanianpour AA. Strength enhancement modeling of concrete cylinders confined with CFRP composites using artificial neural networks. Compos Part B Eng 2012;43(8):2990–3000.

[53] Elsanadedy HM, Al-Salloum YA, Abbas H, Alsayed SH. Prediction of strength parameters of FRP-confined concrete. Compos Part B Eng 2012;43(2):228–39.

[54] Flood I. Towards the next generation of artificial neural networks for civil engineering. Adv Eng Inform 2008;22(1):4–14. https://doi.org/10.1016/j.aei.2007.07.001.

[55] Mangalathu S, Jang H, Hwang S-H, Jeon J-S. Data-driven machine-learning-based seismic failure mode identification of reinforced concrete shear walls. Eng Struct 2020;208:110331. https://doi.org/10.1016/j.engstruct.2020.110331.

[56] Keshtegar B, Nehdi ML, Trung N-T, Kolahchi R. Predicting load capacity of shear walls using SVR-RSM model. Appl Soft Comput 2021;112:107739. https://doi.org/10.1016/j.asoc.2021.107739.

[57] Mansour MY, Dicleli M, Lee JY, Zhang J. Predicting the shear strength of reinforced concrete beams using artificial neural networks. Eng Struct 2004;26(6):781–99. https://doi.org/10.1016/j.engstruct.2004.01.011.

[58] Amani J, Moeini R. Prediction of shear strength of reinforced concrete beams using adaptive neuro-fuzzy inference system and artificial neural network. Sci Iran 2012;19(2):242–8. https://doi.org/10.1016/j.scient.2012.02.009.

[59] Chou J-S, Pham T-P-T, Nguyen T-K, Pham A-D, Ngo N-T. Shear strength prediction of reinforced concrete beams by baseline, ensemble, and hybrid machine learning models. Soft Comput 2020;24(5):3393–411. https://doi.org/10.1007/s00500-019-04103-2.

[60] Chou J-S, Ngo N-T, Pham A-D. Shear strength prediction in reinforced concrete deep beams using nature-inspired metaheuristic support vector regression.

J Comput Civil Eng 2016;30(1):04015002. https://doi.org/10.1061/(ASCE)CP.1943-5487.0000466.
[61] Feng D-C, Wang W-J, Mangalathu S, Hu G, Wu T. Implementing ensemble learning methods to predict the shear strength of RC deep beams with/without web reinforcements. Eng Struct 2021;235:111979. https://doi.org/10.1016/j.engstruct.2021.111979.
[62] Arslan MH. Predicting of torsional strength of RC beams by using different artificial neural network algorithms and building codes. Adv Eng Softw 2010;41(7-8):946–55. https://doi.org/10.1016/j.advengsoft.2010.05.009.
[63] Hwang S-H, Mangalathu S, Shin J, Jeon J-S. Machine learning-based approaches for seismic demand and collapse of ductile reinforced concrete building frames. J Build Eng 2021;34:101905. https://doi.org/10.1016/j.jobe.2020.101905.
[64] Mangalathu S, Hwang S-H, Choi E, Jeon J-S. Rapid seismic damage evaluation of bridge portfolios using machine learning techniques. Eng Struct 2019;201:109785. https://doi.org/10.1016/j.engstruct.2019.109785.
[65] Mangalathu S, Sun H, Nweke CC, Yi Z, Burton HV. Classifying earthquake damage to buildings using machine learning. Earthq Spectra 2020;36(1):183–208. https://doi.org/10.1177/8755293019878137.
[66] Perera R, Arteaga A, Diego AD. Artificial intelligence techniques for prediction of the capacity of RC beams strengthened in shear with external FRP reinforcement. Compos Struct 2010;92(5):1169–75. https://doi.org/10.1016/j.compstruct.2009.10.027.
[67] Tanarslan HM, Secer M, Kumanlioglu A. An approach for estimating the capacity of RC beams strengthened in shear with FRP reinforcements using artificial neural networks. Constr Build Mater 2012;30:556–68. https://doi.org/10.1016/j.conbuildmat.2011.12.008.
[68] Perera R, Tarazona D, Ruiz A, Martín A. Application of artificial intelligence techniques to predict the performance of RC beams shear strengthened with NSM FRP rods. Formulation of design equations. Compos Part B Eng 2014;66:162–73. https://doi.org/10.1016/j.compositesb.2014.05.001.
[69] Abuodeh OR, Abdalla JA, Hawileh RA. Prediction of shear strength and behavior of RC beams strengthened with externally bonded FRP sheets using machine learning techniques. Compos Struct 2020;234:111698. https://doi.org/10.1016/j.compstruct.2019.111698.
[70] Lundberg SM, Lee S. A unified approach to interpreting model predictions. In: 31st conf neural inf process syst. (NIPS 2017), Long Beach, CA, USA; 2017. p. 1–10.
[71] Mangalathu S, Hwang S-H, Jeon J-S. Failure mode and effects analysis of RC members based on machine-learning-based SHapley Additive exPlanations (SHAP) approach. Eng Struct 2020;219:110927. https://doi.org/10.1016/j.engstruct.2020.110927.
[72] Gao X, Lin C. Prediction model of the failure mode of beam-column joints using machine learning methods. Eng Fail Anal 2021;120:105072. https://doi.org/10.1016/j.engfailanal.2020.105072.
[73] Mangalathu S, Shin H, Choi E, Jeon J-S. Explainable machine learning models for punching shear strength estimation of flat slabs without transverse reinforcement. J Build Eng 2021;39:102300. https://doi.org/10.1016/j.jobe.2021.102300.
[74] Wakjira TG, Alam MS, Ebead U. Plastic hinge length of rectangular RC columns using ensemble machine learning model. Eng Struct 2021;244:112808. https://doi.org/10.1016/j.engstruct.2021.112808.
[75] Teng JG, Smith ST, Yao J, Chen JF. Intermediate crack-induced debonding in RC beams and slabs. Constr Build Mater 2003;17(6-7):447–62. https://doi.org/10.1016/S0950-0618(03)00043-6.
[76] Ceroni F, Salzano P. Design provisions for FRCM systems bonded to concrete and masonry elements. Compos Part B Eng 2018;143:230–42. https://doi.org/10.1016/j.compositesb.2018.01.033.
[77] Mandor A, Refai AE. Assessment and modeling of the debonding failure of fabric-reinforced cementitious matrix (FRCM) systems. Compos Struct 2021;275:114394. https://doi.org/10.1016/j.compstruct.2021.114394.
[78] Yu H, Kim S. SVM tutorial-classification, regression and ranking. Handb Nat Comput 2012;1–4:479–506. https://doi.org/10.1007/978-3-540-92910-9_15.
[79] Maalouf M, Homouz D. Kernel ridge regression using truncated newton method. Knowledge-Based Syst 2014;71:339–44. https://doi.org/10.1016/j.knosys.2014.08.012.
[80] Vapnik VN, editor. The nature of statistical learning theory. New York, NY: Springer New York; 1995.
[81] Chang C, Lin C. LIBSVM: a library for support vector machines. ACM Trans Intell Syst Technol 2011;2:1–27. https://doi.org/10.1145/1961189.1961199.
[82] Sutton CD. Classification and regression trees, bagging, and boosting. Handb Stat 2005;24:303–29. https://doi.org/10.1016/S0169-7161(04)24011-1.
[83] Svetnik V, Liaw A, Tong C, Christopher Culberson J, Sheridan RP, Feuston BP. Random forest: a classification and regression tool for compound classification and QSAR modeling. J Chem Inf Comput Sci 2003;43:1947–58. https://doi.org/10.1021/ci034160g.
[84] Friedman JH. Greedy function approximation: a gradient boosting machine. Ann Stat 2001:1189–232. https://doi.org/10.1214/aos/1013203451.
[85] Chen T, Xgboost GC. A scalable tree boosting system. 22nd SIGKDD conference on knowledge discovery and data mining. 2016.
[86] ACI Committee 318, American Concrete Institute. Building code requirements for structural concrete (ACI 318-14): an ACI standard : commentary on building code requirements for structural concrete (ACI 318R-14), an ACI report; 2014.
[87] Wight JK. Reinforced concrete mechanics and design. 7th ed. Hoboken, New Jersey: Pearson Education Inc; 2016.
[88] Szerszen MM, Nowak AS. Calibration of design code for buildings (ACI 318): Part 2 – Reliability analysis and resistance factors. ACI Struct J 2003;100:383–91. https://doi.org/10.14359/12614.
[89] Ruredil. Technical datasheet, Ruredil X mesh C10 data sheet; 2016.